Electronic Structure and Spectroscopy of Oxyallyl: A Theoretical Study

Vadim Mozhayskiy,[†] Daniel J. Goebbert,[‡] Luis Velarde,[‡] Andrei Sanov,[‡] and Anna I. Krylov*,[†]

Department of Chemistry, University of Southern California, Los Angeles, California 90089-0482, and Department of Chemistry and Biochemistry, University of Arizona, Tucson, Arizona 85721-0041

Received: March 10, 2010; Revised Manuscript Received: May 13, 2010

Electronic structure of the oxyallyl diradical and the anion is investigated using high-level ab initio methods. Converged theoretical estimates of the energy differences between low-lying electronic states of oxyallyl (OXA) as well as detachment energies of the anion are reported. Our best estimates of the adiabatic energy differences between the anion $^2A_2$ and the neutral $^3B_2$ and $^3B_1$ states are 1.94 and 2.73 eV, respectively. The $^1A_1$ state lies above $^3B_2$ vertically, but geometric relaxation brings it below the triplet. The two-dimensional scan of the singlet $^1A_1$ potential energy surface (PES) reveals that there is no minimum corresponding to a singlet diradical structure. Thus, singlet OXA undergoes prompt barrierless ring closure. However, a flat shape of the PES results in the resonance trapping in the Franck−Condon region, giving rise to the experimentally observable features in the photoelectron spectrum. By performing reduced-dimensionality wave packet calculations, we estimated that the wave packet lingers in the Franck−Condon region for about 170 fs, which corresponds to the spectral line broadening of about 200 cm^{-1}. We also present calculations of the photodetachment spectrum and compare it with experimental data. Our calculations lend strong support to the assignment of the photoelectron spectrum of the OXA anion reported in Ichino et al. (*Angew. Chem., Int. Ed. Engl.* **2009**, *48*, 8509).

1. Introduction

Diradicals are commonly encountered as reaction intermediates or transition states and are essential in interpreting mechanisms of chemical reactions.[1−4] Following Salem,[5] diradicals are often defined as species with two electrons occupying two (near)-degenerate molecular orbitals (MOs). As an example of a perfect diradical, consider trimethylenemethane (TMM), which has two exactly degenerate (due to symmetry constraints) frontier molecular orbitals (MOs) hosting two unpaired electrons.[6−8] The ground state of TMM is triplet, followed by the singlet states at 1.17 and 3.88 eV (vertically).[9−11] The adiabatic ST gap is 0.699 eV.[10,11] Other diradicals, such as benzynes, metaxylylene, methylene, etc., feature nearly degenerate frontier MOs, and their relative state ordering depends on the energy gap between the frontier MOs as well as their characters, e.g., disjoint versus nondisjoint.[12]

Oxyallyl (OXA) can be viewed as a derivative of TMM in which one CH_2 group is replaced by oxygen.[13] This substitution lowers the symmetry from D_{3h} to C_{2v} lifting the degeneracy between the frontier MOs and stabilizing the singlet state. However, the differences in electronic structure between TMM and OXA are more substantial. The lone pairs on oxygen give rise to a second diradical manifold, which can interact with the TMM-like states. This is similar to other oxygen-containing diradicals, such as Cvetanvič diradicals produced by reactions of atomic or molecular oxygen with unsaturated hydrocarbons.[14−17]

Figure 1 shows relevant MOs of OXA. The a_2 and three b_1 orbitals are of π-like character and can be described as the distorted TMM orbitals.[9] The lowest b_1 orbital, which is predominantly an out-of-plane oxygen's lone pair, lies below two other b_1 orbitals derived from carbon's p_z, in agreement with electronegativity considerations. However, above the lowest b_1, there is a b_2 orbital corresponding to the in-plane oxygen lone pair. This orbital gives rise to several electronic configurations (and low-lying electronic states), which are unique for OXA.

Figure 2 shows electronic configurations of the ground state of the OXA anion and the three lowest electronic states of the OXA diradical (see section 2). While the lowest triplet and singlet states, $^3B_2$ and $^1A_1$, are derived from different distributions of two electrons over the TMM-like a_2 and b_1 MOs, the next electronic state, $^3B_1$, has the unpaired electron on the in-plane oxygen lone pair, b_2. Different distributions of the two electrons on the a_2 and b_2 orbitals give rise to another manifold of diradical states.

Electronic structure calculations of diradicals are challenging due to multiconfigurational character of the wave functions and small energy gaps between states which require high accuracy and balanced description of multiple states.[18] The most reliable approach is the equation-of-motion spin-flip coupled-cluster (EOM-SF-CC) method that describes target diradical states as spin-flipping excitations from a well behaved high-spin reference.[18−22] The SF method describes all target states on an equal footing, includes dynamical and nondynamical correlation in a single computational step and does not involve active space selection and state averaging. When the CCSD (or OO−CCD) wave function is used as the reference, the typical errors in energy differences are 0.1 eV, and perturbative inclusion of triple excitations brings the errors below 1 kcal/mol (0.05 eV),[21] provided that an adequate basis set is employed. The calculations become even more challenging when other electronic states (e.g., second diradical manifold, anionic states) are important. To accurately compute energy differences between multiple states of different character, one needs to employ appropriate computational strategies with built-in error cancellations (rather than rely on a brute-force approach), which can be achieved by judicious combination of different CC and EOM-CC methods.[23−25]

[†] University of Southern California.
[‡] University of Arizona.

10.1021/jp102183z
Published on Web 06/15/2010

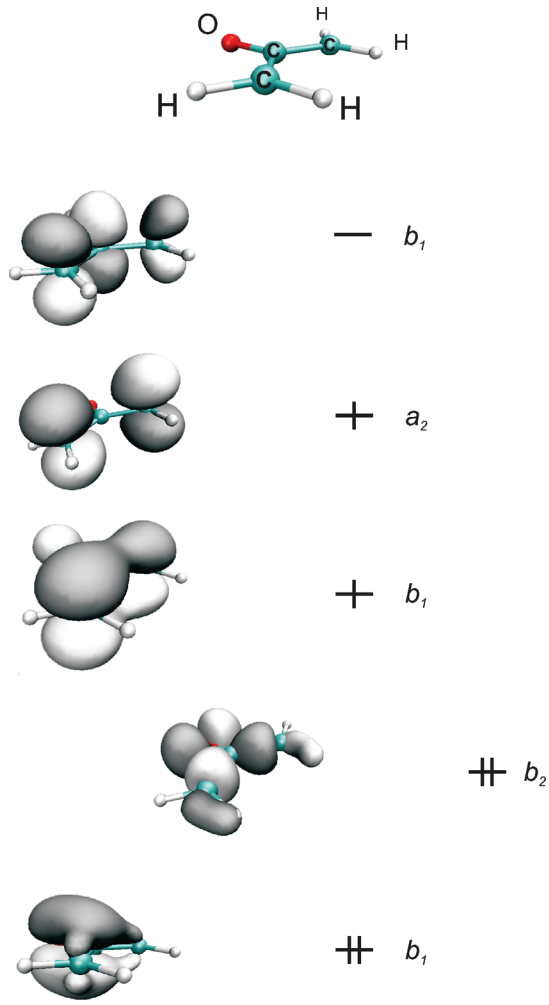

Figure 1. Frontier MOs of OXA. Electronic configuration of the triplet $^3B_2$ state is shown. Orientation of the molecule is shown at the top.

Although OXA has been postulated as a reactive intermediate in several classes of organic reactions, its experimental characterization has proven to be difficult, a possible reason being facile ring closure forming cyclopropanone (for a brief history, see ref 26).

The results of the neutralization−reionization mass spectrometric study, which attempted to produce neutral OXA from the anion, have not provided sufficient evidence of the production of the neutral.[27]

The first direct experimental observation of OXA via photodetachment of the oxyallyl anion was reported recently.[13] The authors presented the photoelectron spectrum and assigned the observed progressions to the $^3B_2$ and $^1A_1$ states of neutral oxyallyl. These results play a crucial role in framing the theoretical work present here. For the first time, theoretical exploration of this challenging system benefits from a much needed and long awaited, solid experimental reference. In particular, the experiment of Ichino et al.[13] not only yielded the electron binding energies (eBEs) of the $^3B_2$ and $^1A_1$ states of OXA (1.997 ± 0.010 and 1.942 ± 0.010 eV, respectively) but also showed the extensive peak broadening for the singlet state, which may be interpreted as due to transition state dynamics.

The previous theoretical studies of OXA provide a stark demonstration of methodological challenges posed by diradicals.[28,29,27,30−33,13] For example, the reported values of singlet−triplet (ST) gap vary from −0.22 to +0.87 eV. The answers to another important question, whether or not the singlet OXA diradical can be isolated (i.e., whether there is a minimum on the singlet potential energy surface corresponding to an open-ring diradical structure) also vary wildly. This frustrating for theory situation is reflected in the most recent study,[13] which reports a collection of calculated detachment energies ranging from 1.68 to 2.08 eV.

The purpose of our study is to provide reliable theoretical description of the important aspects of the electronic structure of OXA. The failure of theory to yield converged and accurate results for OXA is not at all surprising owing to the nature of methods employed in previous studies. Indeed, DFT (and broken-symmetry DFT) is not capable of even giving a qualitatively correct description of the diradical wave functions. Moreover, self-interaction error often spoils the treatment of radicals (especially charged ones).[34−36] The multireference methods employ more appropriate wave functions; however, obtaining quantitative results is difficult due to a subtle balance between dynamical and nondynamical correlation energy, arbitrariness in active space selection, etc. Additional difficulties arise due to uncertainties in equilibrium geometries, i.e., bare CASSCF geometries often employed in energy calculations using higher level methods are rather crude (see, for example, ref 9), which may introduce additional errors in small energy gaps. Moreover, the selection of the active space for CASSCF strongly influences the shape of the PES even on the CASPT2 level, e.g., in a study of tetramethylene some stationary points calculated at the lower level of theory disappeared in more accurate calculations.[37] Finally, basis sets much larger than used in the previous studies are required for converged results, as demonstrated below.

We report accurate equilibrium geometries and the converged values of detachment energies and energy gaps between the low-lying OXA states. Our best estimates of the adiabatic energy differences (including the zero-point energies, ZPE) between the anion $^2A_2$ and the neutral $^3B_2$ and $^3B_1$ states are 1.94 and 2.73 eV, respectively. At the equilibrium geometry of the anion, the $^1A_1$ state lies above $^3B_2$, but geometry relaxation brings the singlet below the triplet. We also present scans of the singlet $^1A_1$ PES, demonstrating that there is no minimum corresponding to a singlet diradical structure. Thus, singlet OXA undergoes prompt barrierless ring closure. However, a flat shape of the PES results in the resonance trapping on the singlet PES giving rise to the experimentally observable features in the photoelectron spectrum. Using reduced-dimensionality wave packet calculations, we estimated that the wave packet lingers in the Franck−Condon region for about 170 fs, which corresponds to the spectral line broadening of about 200 cm^{-1}.[38] We also present calculations of the photodetachment spectrum and compare it with experimental results.[13,39]

2. Theoretical Methods and Computational Details

Reliable calculations of energy differences between multiple electronic states of different character require appropriate computational strategies that are based on balanced description of different states and have built-in error cancellation (see, for example, refs 24 and 25), in the spirit of isodesmic reactions.[40]

Figure 3 shows electronic configurations of the low-lying states of OXA and its anion. The wave functions of the doublet anion and high-spin neutral triplet states are of single-configurational character and can be well described by the ground state coupled-cluster methods, i.e., CCSD. Chemical accuracy can be achieved by including triples corrections, e.g., within CCSD(T)[41,42] or CCSD(dT).[21,43] To mitigate possible

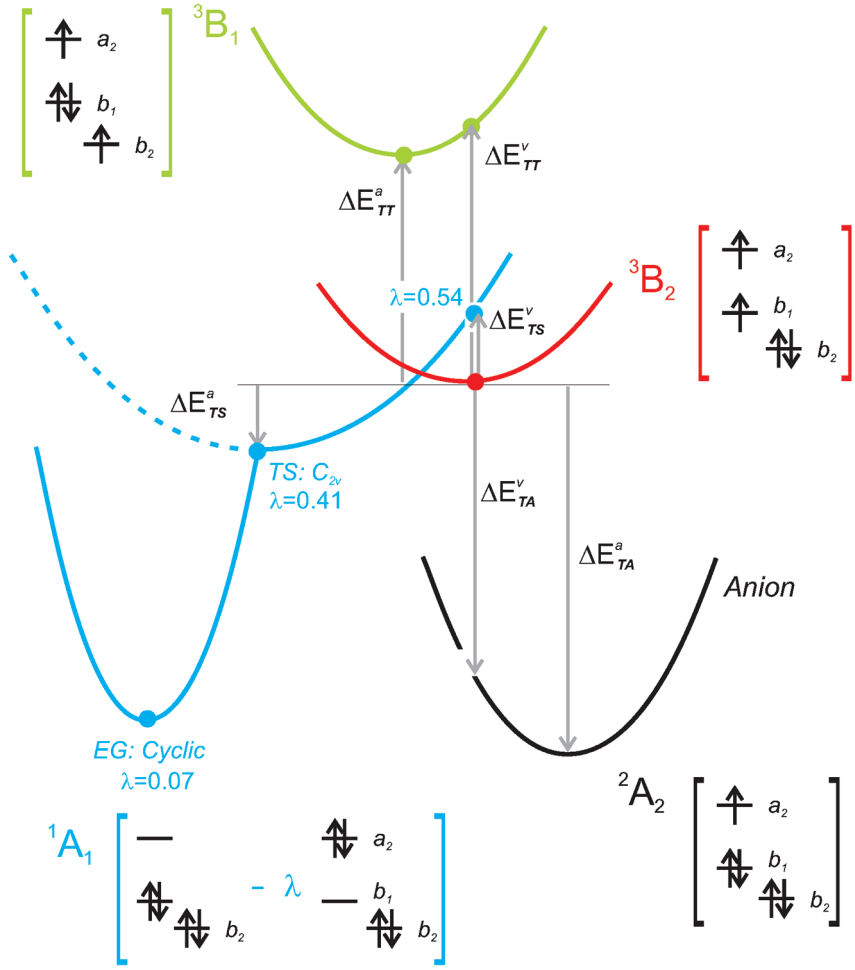

Figure 2. Lowest electronic states of OXA. The $^3B_2$ state has a open-ring C_{2v} minimum, whereas the optimized C_{2v} structure of the $^1A_1$ state is a transition state (TS). The vertical and adiabatic energy differences of the anion and singlet TS relative to the triplet $^3B_2$ state are given in Tables 1−3. The second leading wave function amplitudes, λ, are also shown.

effects of spin-contamination, ROHF references are employed throughout this study. Energy differences between these states can be computed as differences between the respective total CCSD(T) or CCSD(dT) energies.[24,25]

The $^1A_1$ and $^1B_2$ states have multiconfigurational wave functions that can be described by EOM-SF[22] from the high-spin $^3B_2$ reference. Note that some of the configurations of the $^1B_2$ state appear as double excitations from $^3B_2$, and therefore, we anticipate larger errors for this state.

The states that are derived from the $^3B_1$ manifold (shown on the right side of Figure 3 can be described by SF from that reference. Alternatively, both $^3B_2$ and $^3B_1$ (as well as higher $^3B_2$) can be described by EOM-CC for ionized states, EOM-IP,[44−49] using the $^2A_2$ reference.

Finally, the energy gap between $^2A_2$ and $^3B_2$ can also be computed by EOM-CC for electron attachment, EOM-EA,[44,50] from the $^3B_2$ reference. Note that the EOM-EA operator in this case corresponds to attaching of a β rather than an α electron, as was done in the study of *p*-benzyne anion.[51]

We also characterized electronically excited states of the anion using EOM-EE-CCSD/6-311(+,+)G(2df,2pd). The lowest excited state corresponds to the $b_1 \rightarrow a_2$ excitation and is 1.4 eV vertically. The next excited state lies at 2.5 eV. It corresponds to $b_2 \rightarrow a_2$ excitation and has low (but not negligible) oscillator strength ($f_l = 0.013$) owing to its lp $\rightarrow \pi^*$ character. This state is above the onset of the detachment continuum and, therefore, is of resonance character. Photoexcitation to this state will result in autodetachment and thus can contribute to the photoelectron signal above 2.5 eV.

As demonstrated by the numeric results below, the energy differences are extremely sensitive to the correlation treatment and basis set selection, and a balanced description of the relevant states is crucial for obtaining accurate results.

Calculation of adiabatic energy differences requires accurate equilibrium geometries. The $^2A_2$ (anion) and $^3B_2$ state equilibrium geometries were optimized by CCSD/6-311(+,+)G(2df,2pd) using UHF reference. The planar C_{2v} structure of the $^1A_1$ state was optimized by EOM-SF-CCSD/6-311(+,+)G(2df,2pd). This structure is not a minimum but a transition state (TS) with a 203 cm^{-1} imaginary frequency for out of plane symmetric rotation of the CH_2 groups. The $^3B_1$ equilibrium geometry was computed by EOM-IP-CCSD/6-311(+,+)G(2df,2pd).

To investigate the reaction coordinate for ring closure, we performed two-dimensional scans of the $^1A_1$ PES, along the CCC angle and out-of-plane symmetric rotation of the CH_2 groups. The reaction path is well described in these two internal coordinates, but some minor relaxation of bond lengths and tilting of CO out of CCC plane (at the beginning of cyclization) is ignored. Note that relaxing other degrees of freedom along the reaction coordinate would only lower the energy and reduce the barriers connecting the fully optimized reactant structure and the product well. z-matrix parameters for this 2D scan are given in the Supporting Information.

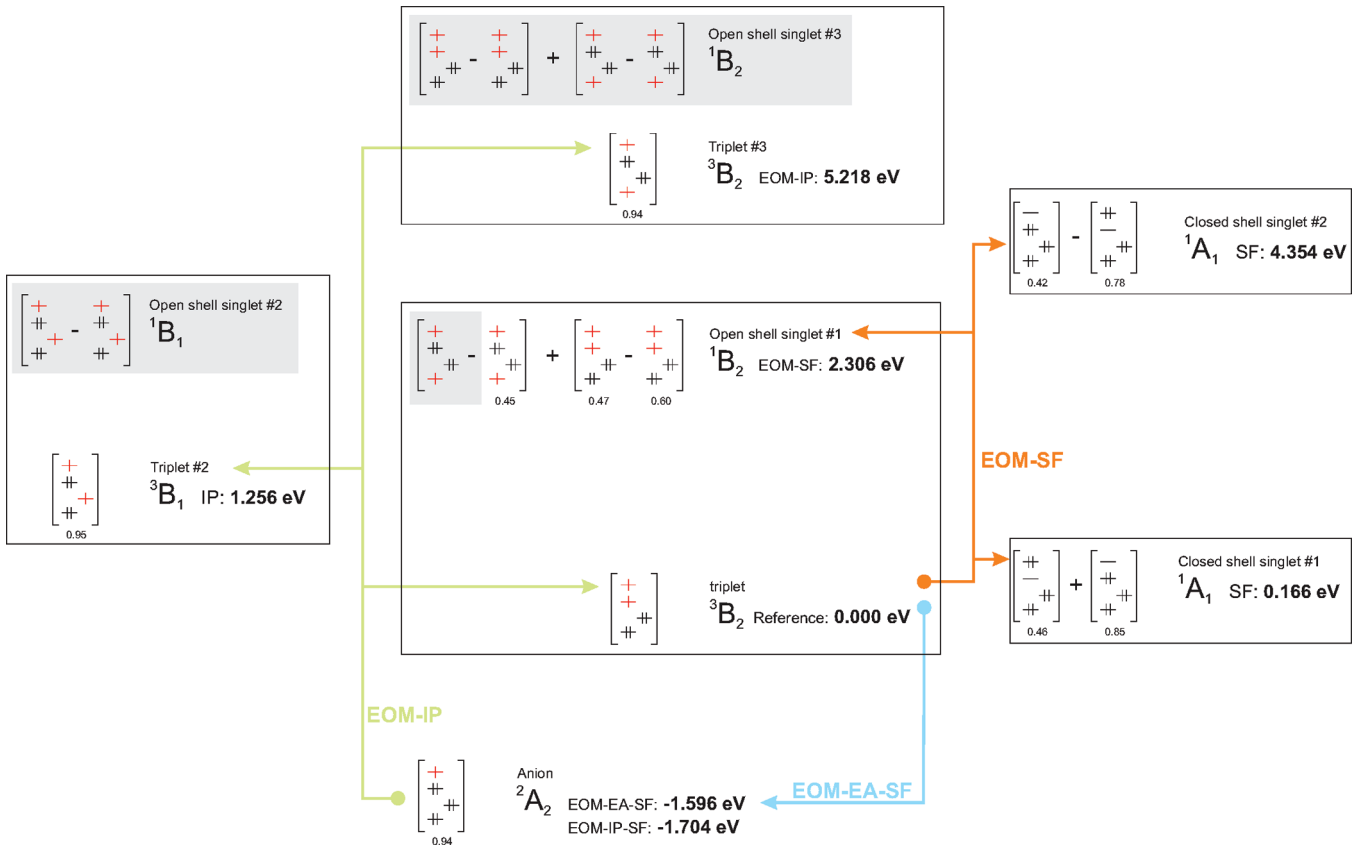

Figure 3. Electronic states of neutral OXA and its anion. Vertical energy differences are relative to the $^3B_2$ triplet state at its equilibrium geometry. The weights of leading electronic configurations as given by the EOM wave functions are shown. The two $^1A_1$ and $^1B_2$ states (right) are described by EOM-SF-CCSD(dT) from a $^3B_2$ reference. The two $^3B_2$ and $^3B_1$ are described by EOM-IP from $^2A_2$. The anion−triplet (lowest $^3B_2$) energy gap is calculated by EOM-EA and EOM-IP from triplet and anion references, respectively. The shaded configurations are not well described. All EOM-CCSD calculations employed ROHF references and the 6-311(+,+)G(2df,2pd) basis set.

This PES was used for the wave packet propagation to investigate resonance trapping in the Franck−Condon region. Ab initio 2D PES calculated on the 24 × 16 grid was interpolated using a natural cubic spline on the 200 × 200 rectangular uniform grid. The Fourier method[52,53] was used for the discrete representation of the Hamiltonian. The time-dependent Schrödinger equation was solved using the split-operator method[54] with a 6 attosecond (0.25 atomic time units) time step. The initial wave function at $t = 0$ was represented by a 2D Gaussian corresponding to the ground vibrational state of the anion in the harmonic approximation, i.e., the product of two 1D Gaussians with 449 cm^{-1} (CCC-bend) and 411 cm^{-1} (CH_2 out of plane rotation) frequencies. This initial wave function was displaced by 0.12 (3.3°) along the mass-weighted CCC-bend normal mode. The absorbing boundary conditions[55] were used to dump the reflections from the boundaries resulting in a slow decay of the wave function norm to 0.9998 and 0.87 at 200 fs and 2 ps, respectively.

The photoelectron spectrum of the anion ($^2A_2$) was computed using double harmonic approximation with Duschinskii rotations with *ez*Spectrum.[56] Equilibrium geometries and frequencies were computed by CCSD/6-311(+,+)G** ($^2A_2$ and $^3B_1$), EOM-SF-CCSD/6-31G* ($^1A_1$), and EOM-IP-CCSD/6-31G* ($^3B_2$). For the singlet transition state, planar C_{2v} structure was used and the imaginary frequency was ignored. Such approach can be used to approximately describe a vibrational resonance.

All electronic structure calculations were performed using *Q*-Chem electronic structure program.[57] The relevant geometries, energies, and frequencies are given in the Supporting Information.

TABLE 1: Vertical Energy Gaps (eV) Relative to the Triplet State at Its Equilibrium Geometry Calculated with Different Basis Sets[a]

	ΔE^v_{TA} CCSD(T)	ΔE^v_{TS} EOM-SF-CCSD(dT)
6-311G**	−0.987	0.164
6-311(+,+)G**	−1.501	0.111
6-311(2+,2+)G**	−1.505	0.112
6-311(+,+)G(2df,2pd)	−1.714	0.071
6-311(+,+)G(3df,3pd)	−1.767	0.063
cc-pVTZ	−1.420	0.101
aug-cc-pVDZ	−1.680	0.061
aug-cc-pVTZ	−1.803	0.061

[a] E_{TA} and E_{TS} denote triplet−anion and triplet−singlet energy separations, respectively.

3. Results and Discussion

3.1. Vertical and Adiabatic Electronic State Ordering. Tables 1−3 show vertical and adiabatic energy gaps between the anion ($^2A_2$) and the neutral $^3B_2$, $^1A_1$ (planar TS), and $^3B_1$ states (see Figure 2). Additional calculations are given in the Supporting Information. Our best estimate of the adiabatic detachment energy (DE or eBE) of the anion corresponding to photodetachment to the $^3B_2$ state is 1.89 eV (DE_{ee}, i.e., no ZPE). The best value for the singlet−triplet (ST) gap (using planar TS structure of the $^1A_1$ state) is −0.063 eV (the singlet state being below the triplet). Our best estimate of the $^3B_2$−$^3B_1$ adiabatic gap (no ZPE) is 0.77 eV,[58] which yields 2.66 eV for the $^2A_2$−$^3B_1$ gap.

These energy gaps are very sensitive to the methods employed. To quantify this dependence, we analyze vertical

TABLE 2: Vertical (E^v_{TA}) and Adiabatic (E^a_{TA}) Energy Differences (eV) of the Anion Relative to the Lowest Triplet State[a]

	EOM-EA-SF-CCSD	EOM-IP-CCSD	ΔCCSD(dT)	ΔCCSD(T)
vertical, E^v_{TA}	−1.654	−1.769	**−1.784**	−1.803
relaxation energy	−0.092	−0.101	−0.102	−0.101
adiabatic, E^a_{TA}	−1.746	−1.870	**−1.886**	−1.904

[a] The best theoretical estimates are shown in bold. Energies are obtained with the aug-cc-pVTZ basis set.

TABLE 3: Vertical (E^v_{TS}) and Adiabatic (E^a_{TS}) Energy Gaps (eV) between the Singlet (Planar TS Structure) and the Triplet States[a]

	ΔCCSD(T)	EOM-SF-CCSD	EOM-SF-CCSD(dT)
E^v_{TS}	0.249	0.155	**0.061**
relaxation energy	−0.154	−0.153	−0.124
E^a_{TS}	0.095	0.002	**−0.063**

[a] The best theoretical estimates are shown in bold. Energies are obtained with the aug-cc-pVTZ basis set.

energy gaps, i.e., DEs at a fixed nuclear geometry. Table 1 demonstrates the basis set dependence of the vertical energy gap between (i) the lowest triplet state and the ground state of the anion and (ii) the lowest singlet and the lowest triplet states. These energy differences are computed at the equilibrium geometry of the triplet state. The gaps in Table 1 are computed by the most appropriate correlation methods. The gaps are very sensitive to the basis set size, and the converged values require the basis of an aug-cc-pVTZ quality (e.g., ΔE^v_{TA} changes by 0.4 eV upon adding diffuse functions to the cc-pVTZ basis). The anion−triplet gap converges slower than the ST gap. For example, the difference in ΔE^v_{TA} in the Pople and Dunning triple-ζ bases is 0.4 eV, whereas the difference between the respective ΔE^v_{ST} is only 0.06 eV. This is because ΔE^v_{TA} is computed by the ΔE approach,[59] which relies on converged total energies. Thus, nondynamical correlation should be recovered, which requires large basis sets. Moreover, diffuse functions are more important for the anion than for the neutral. Our best estimates of the ΔE^v_{TA} and ΔE^v_{TS} are −1.784 and +0.061 eV, respectively, obtained at the CCSD(dT)/aug-cc-pVTZ and EOM-SF-CCSD(dT)/aug-cc-pVTZ levels.

Tables 2 and 3 present vertical versus adiabatic energy gaps between the anion and the two lowest states of the neutral (see Figure 2). The vertical gaps are computed at the equilibrium geometry of the triplet state. As one can see, the gaps are also sensitive to the correlation treatment. While EOM-CCSD methods provide balanced description of the states involved, the effect of triples excitation is important for the quantitative accuracy.

As Tables 2 and 3 show, structural relaxation (under C_{2v} constraint) brings the singlet $^1A_1$ state below the triplet $^3B_2$. Our best estimate of the adiabatic singlet−triplet and anion-triplet gaps are 0.063 and 1.886 eV, respectively (obtained at the EOM-SF-CCSD(dT)/aug-cc-pVTZ and the CCSD(dT)/aug-cc-pVTZ levels). However, as shown below, the planar singlet structure is not a true minimum but a TS. The true minimum of the $^1A_1$ state corresponding to the closed-ring structure is of course much lower, i.e., 1.71 eV below $^3B_2$ as computed with CCSD/6-311(+,+)G(2df,2pd) (no ZPE).

3.2. Equilibrium Geometries and Vibrational Frequencies. Figure 4 shows optimized structures of the anion's $^2A_2$ state, singlet $^1A_1$, and triplet $^3B_2$. In all three states, the geometry

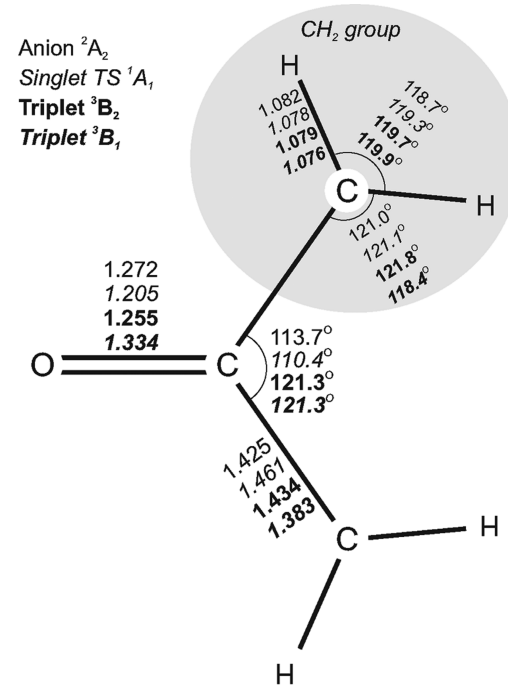

Figure 4. Bond lengths (Å) and angles (degree) of the C_{2v} optimized structures of the $^2A_2$, $^1A_1$, $^3B_2$, and $^3B_1$ states shown in normal, italic, bold, and bold italic fonts, respectively. The planar C_{2v} structure of $^1A_1$ is not a minimum but a transition state (TS).

of the CH_2 groups is approximately the same, and only three internal coordinates show large differences between the states, i.e., the CCC angle and the CC and CO bonds. Thus, we expect the following two normal modes to be active in the photoelectron spectrum: (i) bending mode in the CCC angle and (ii) symmetric stretching mode, which simultaneously shortens the CO bond and stretches both CC bonds.

The triplet $^3B_2$ state is displaced mostly along the bending normal mode relative to the anion, and the optimized singlet structure, which is a transition state, differs from the anion along the CO/CC stretching normal mode. This is consistent with the MOs: the triplet and singlet states are derived by removing an electron from the orbitals that are of bonding and antibonding character with respect to the two radical centers, respectively. The b_1 orbital is antibonding along the CO bond. The $^3B_1$ state, which is derived by removing the electron from the in-plane oxygen lone pair orbital that also has anti bonding character along the CC bonds, has the longest CO and the shortest CC bonds.

Frequencies of these states are shown in Table 4. In agreement with the MO considerations, the largest changes are observed in the CO and CC stretches. Relative to the anion, the former increases in the singlet and decreases in both triplets. The CC stretch becomes softer in $^3B_2$ and stiffer in $^3B_1$.

3.3. Transient Singlet OXA Structure and Its Spectroscopic Signatures. The true equilibrium geometry of the singlet $^1A_1$ state is the cyclic structure with the CCC angle of 64.6°, CC bond 1.474 Å, and CO bond 1.197 Å; adiabatically it is 1.75 eV below the triplet $^3B_2$ state. The cyclic equilibrium geometry is derived from the TS $^1A_1$ structure by closing the CCC angle and rotating the CH_2 groups out of the molecular plane. Figure 5 shows the PES scan of the $^1A_1$ state in these two coordinates. As one can see, there is no barrier separating the Franck−Condon region (which is close to the planar OXA TS) and the cyclic cyclopropanone structure. The potential along the reaction coordinate is extremely shallow near the planar

TABLE 4: Frequencies (cm^{-1}) for the $^2A_2$, $^1A_1$, $^3B_2$, and $^3B_1$ States Calculated with the 6-31G* Basis Set[a]

		anion $^2A_2$ CCSD		singlet $^1A_1$ TS EOM-SF-CCSD		triplet $^3B_2$ CCSD		triplet $^3B_1$ EOM-IP-CCSD	
sym CH_2 OP	b_1	411	*(12)*	−203		431	*(1.5)*	486	*(3.4)*
sym CH_2 OP	b_1	433	*(90)*	475	*(19)*	724	*(83)*	694	*(118)*
asym CH_2 OP	a_2	436	*(0.0)*	774	*(0.0)*	644	*(0.0)*	720	*(0.0)*
CCC bend.	a_1	449	*(0.0)*	398	*(9.5)*	409	*(0.9)*	404	*(0.3)*
CO tilt	b_2	468	*(33)*	500	*(33)*	524	*(3.4)*	462	*(41)*
CH stretch	a_2	561	*(0.0)*	473	*(0.0)*	321	*(0.0)*	604	*(0.0)*
CO bend. OP	b_1	692	*(22)*	771	*(79)*	540	*(9.6)*	643	*(6.4)*
asym CH_2 tilt	b_2	925	*(115)*	925	*(12)*	961	*(1.3)*	987	*(1.7)*
sym CC stretch	a_1	961	*(1.2)*	882	*(21)*	914	*(2.0)*	1040	*(0.3)*
sym CH_2 tilt	a_1	1069	*(28)*	1090	*(8.7)*	1082	*(4.3)*	937	*(20)*
asym CC stretch	b_2	1079	*(958)*	1300	*(53)*	1356	*(51)*	1295	*(20)*
asym HCH bend.	b_2	1480	*(47)*	1506	*(37)*	1519	*(52)*	1498	*(16)*
sym HCH bend.	a_1	1494	*(18)*	1508	*(7.9)*	1503	*(0.7)*	1525	*(12)*
CO stretch	a_1	1613	*(331)*	1902	*(367)*	1421	*(0.1)*	1414	*(30)*
CH stretch	b_2	3131	*(116)*	3197	*(0.2)*	3197	*(0.2)*	3230	*(3.4)*
CH stretch	a_1	3144	*(20)*	3203	*(0.0)*	3201	*(6.7)*	3229	*(0.0)*
CH stretch	b_2	3221	*(37)*	3311	*(0.8)*	3309	*(0.2)*	3340	*(0.3)*
CH stretch	a_1	3229	*(88)*	3316	*(6.4)*	3312	*(4.6)*	3340	*(3.8)*
				Zero Point Energy, eV					
6-31G*		1.53		1.58		1.57		1.60	
6-311(+,+)G**		1.49		1.55		1.55		1.57	

[a] IR intensities are shown in parentheses. OP: out-of-plane vibrations, the rest are in plane vibrations.

OXA geometries (small CH_2 out of plane rotation angles).[60] Thus, the singlet OXA diradical is not a stable species in the gas phase. However, the flat shape of PES suggests the finite lifetime of the wave packet in the Franck−Condon region (or, in other words, trapping in a vibrational resonance), which can give rise to a band in the photoelectron spectrum. We observed such behavior in our recent study of the photoelectron spectrum of water dimer cation, where the wave packet calculations showed that the wave packet lingers on the shelf in the Franck−Condon region despite large structural differences between the neutral and the ionized equilibrium geometries.[61]

To evaluate the lifetime of the wave packet in the Franck−Condon region, we performed 2D wave packet propagation on the singlet PES. Figure 6 shows wave packet snapshots and the autocorrelation function.

We observe that the wave packet spends about 100 fs in the Franck−Condon region. At about 250 fs, the autocorrelation function approaches zero and the OXA structure can be described as a closed-ring one. The expectation values of CCC and CH_2 are equal to 97° and 50°, respectively; however, the wave packet is rather delocalized, as shown in Figure 6d. Since energy redistribution between the vibrational modes (IVR) cannot be correctly described by this two-dimensional model, the autocorrelation function exhibit multiple recurrences up to about 2 ps. One can expect that coupling with 16 remaining degrees of freedom will efficiently dissipate the vibrational energy from the reaction coordinate making the return of the wave packet from the bottom of the well back to the Franck−Condon region unlikely. Thus, we estimate the lifetime in the Franck−Condon region as 170 fs. This corresponds to 10 CO vibrations (the frequency of the CO/CC stretch is 1902 cm^{-1}, which yields 17.5 fs for one vibrational period) and approximately 200 cm^{-1} line broadening.[38] Thus, CO/CC progression of the singlet PES may be observed in the experimental spectrum.

3.4. Photoelectron Spectrum of the OXA Anion. Figure 7 shows the experimental[13,39] and theoretical photoelectron spectra of the OXA anion. The theoretical spectrum was computed using the double harmonic approximation with Duschinskii rotations,

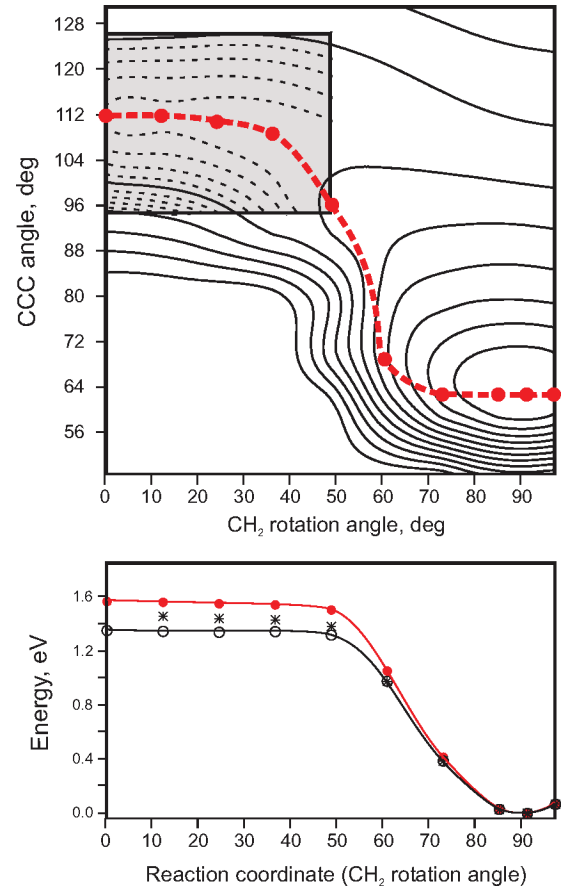

Figure 5. Top panel: PES scan of the singlet $^1A_1$ surface (EOM-SF-CCSD/6-31G*, UHF). Solid and dashed contour lines are every 0.25 and 0.05 eV, respectively. The red dashed line denotes the approximate reaction path from the C_{2v} transition state (0, 112) to the equilibrium cyclic geometry (90, 64). Geometry of the "C_s transition state" discussed in ref 13 is close to the (35, 108) point on this plot. Bottom panel: PES scan along the reaction path from the top panel (solid red circles) EOM-SF/6-31G*, UHF; (stars) EOM-SF/6-311(+,+)G(2df,2pd), UHF; (empty black circles) EOM-SF/6-311(+,+)G(2df,2pd), ROHF.

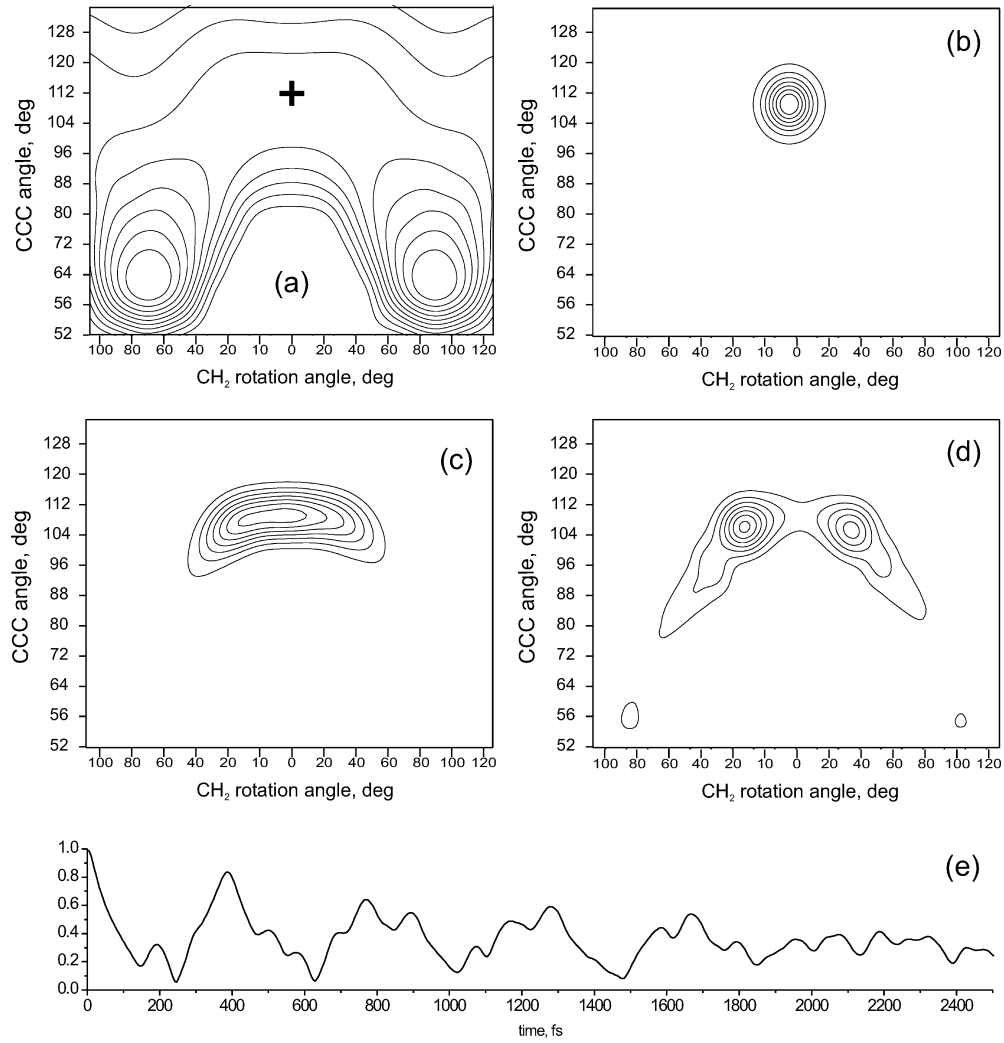

Figure 6. Evolution of the anion ground vibrational state wave function on the singlet $^1A_1$ PES. (a) Two-dimensional PES with contour lines every 0.27 eV. The cross marks the Franck−Condon region. (b) Initial wave function shown with contour interval 0.2. (c) and (d) Wave packet at time $t = 55$ fs and $t = 110$ fs, respectively. The autocorrelation function is shown in (e).

as described in section 2. As follows from Figure 4, the anion−triplet ($^2A_2 \rightarrow {}^3B_2$) photodetachment transition activates the CCC-bending normal mode, leading to an extended vibrational progression with the peak spacing of 409.2 cm^{-1} [computed at the CCSD/6-311(+,+)G** level]. Figure 7a shows the photoelectron spectrum of the OXA anion computed considering the $^3B_2$ neutral state only. In this case, the origin of the $^2A_2 \rightarrow {}^3B_2$ transition is set at eBE = 1.95 eV, coinciding with the position of the first peak in the experimental spectrum. For comparison, the best theoretical value (including the ZPE correction) for the $^2A_2 \rightarrow {}^3B_2$ origin transition is 1.94 eV. The calculated peak positions in Figure 7a agree very well with the experimental progression; however, the relative intensities (calculated as Franck−Condon factors squared) of the second and third peak are reversed. This discrepancy suggests that the computed spectrum does not take into account all active transitions. Moreover, the polarization measurements and observed peak broadening have suggested that the first peak belongs to the singlet state.[13,39] As discussed above, the very flat PES of the $^1A_1$ state along the reaction coordinate toward ring closure (which corresponds to the symmetric out-of-plane rotation of the two CH_2 groups) gives rise to a relatively long lifetime (170 fs) of the initial wave packet in the Franck−Condon region. Thus, the singlet state is expected to contribute well-defined vibrational lines to the photoelectron spectrum. The most active normal mode in photoexcitation from the anion to the $^1A_1$ transition state is the CO/CC stretching normal mode, with the frequency 1902 cm^{-1} (at the EOM-SF-CCSD/6-31G* level). Figure 7b shows the photoelectron spectrum in the same energy range as before, computed with the contributions of both the $^3B_2$ and $^1A_1$ neutral states. Compared to peaks in Figure 7a, the origin of the $^3B_2$ band is now shifted to 2.01 eV, to coincide with the position of the second peak in the experimental spectrum, while the first peak, at eBE = 1.95 eV, is assigned as the origin of the $^1A_1$ band. For comparison, the best theoretical estimate (including the ZPE correction) for the singlet 0−0 transition is 1.88 eV. The $^1A_1$ band intensities in the theoretical spectrum are multiplied by 0.3 relative to the $^3B_2$ state. Due to accidental degeneracy between the $^1A_1 \rightarrow {}^3B_2$ energy gap and the CO/CC progression in the triplet state, the calculated peak positions in Figure 7b agree with the experiment just as well as in Figure 7a. In addition, the relative intensities of the second and third peak in the combined $^3B_2$ and $^1A_1$ spectrum also agree with the experiment. It is troublesome that the second peak in the singlet state progression in Figure 7b (at eBE = 2.19 eV) is not as prominent as expected in the experimental spectrum, but the resonance character of the $^1A_1$ state may be responsible for this behavior. Indeed, the experimental spectrum reported in ref 13 exhibits a broadened peak corresponding to the

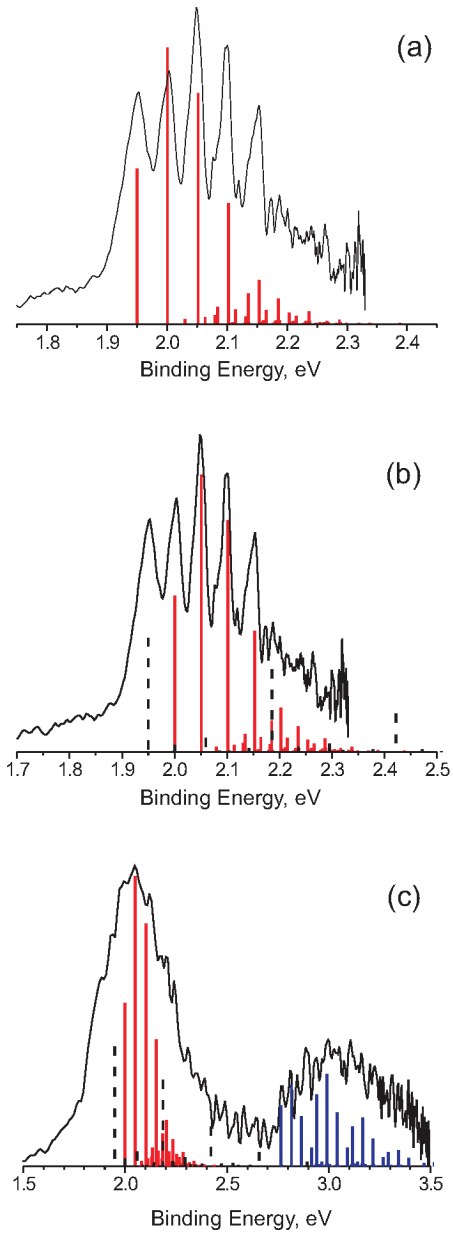

Figure 7. Calculated (see section 2) and experimental[13,39] photoelectron spectrum of the OXA anion. Solid red, dashed black, and solid blue bars denote the progressions in the triplet $^3B_2$, singlet $^1A_1$, and triplet $^3B_1$ bands, respectively. Solid black lines are the experimental photoelectron spectra[13,39] measured with 532 nm (a), (b) and 355 nm (c) lasers. (a) The calculated triplet state progression is superimposed with the experimental spectrum. (b), (c) The calculated singlet and triplet state progressions are shifted such that their respective 00 lines coincide with the positions of the first and the second peak.

fundamental level of the CO stretching mode. Thus, the overall agreement between the experimental and calculated spectra, combined with the polarization dependence of the relative peak intensities and observed broadening of the singlet lines[13] make the reported assignment convincing. Figure 7c shows the theoretical and experimental photoelectron spectra of OXA^- up to eBE = 3.5 eV. The origin of the $^3B_1$ band is shifted to 2.77 eV, compared to the computed value of 2.73 eV, based on the ZPE corrected adiabatic $^3B_2 \rightarrow {}^3B_1$ gap of 0.80 eV. The $^2A_2 \rightarrow {}^3B_1$ band intensities in Figure 7c are multiplied by 0.6 relative to the $^3B_2$ band. The individual vibrational lines correspond to the CO/CC stretch and CCC bend progressions in the $^3B_1$ state. The overall shape of the $^3B_1$ band agrees well; however, the experimental resolution is not sufficient to assign the individual peaks of these progressions.

4. Conclusions

We have reported accurate electronic structure calculations of the low-lying electronic states of oxyallyl and oxyallyl anion. Our best estimates for the adiabatic electron binding energies (including ZPE) corresponding to the $^3B_2$ and $^3B_1$ neutral states are 1.94 and 2.73 eV, respectively, compared to the reported experimental values are 2.01 and 3.02 eV. The electron binding energy of the neutral $^1A_1$ at the relaxed geometry of the anion is calculated to to be 1.88 eV, compared to the experimental value of 1.942 eV. However, the singlet PES does not have a minimum corresponding to an open-ring diradical structure. Thus, the singlet diradical is not a stable species in the gas phase and undergoes barrierless isomerization to the cyclopropanone. The flat shape of the PES suggests resonance trapping in the Franck−Condon region giving rise to a feature in the photoelectron spectrum. The estimated lifetime is 170 fs, which corresponds to 200 cm^{-1} line width. Thus, our calculation lend strong support to the reported assignment of the photodetachment spectra of the OXA anion.

Acknowledgment. This work is conducted under auspices of the *i*OpenShell Center for Computational Studies of Electronic Structure and Spectroscopy of Open-Shell and Electronically Excited Species supported by the National Science Foundation through the CRIF:CRF CHE-0625419 + 0624602 + 0625237 grant. A.I.K. also acknowledges support of the Department of Energy (DE-FG02-05ER15685). A.S. acknowledges support of the National Science Foundation (CHE-0713880). We thank Prof. W. C. Lineberger for stimulating discussions and insightful comments on this manuscript prior the publication.

Supporting Information Available: Lists of optimized geometries and z-matrix parameters. This material is available free of charge via the Internet at http://pubs.acs.org.

References and Notes

(1) Turro, N. *Modern Molecular Photochemistry*; Benjamin/Cummings Publishing Co.: Menlo Park, CA, 1978.
(2) Borden, W. T., Ed. *Diradicals*; Wiley: New York, 1982.
(3) Bonaćič-Koutecký, V.; Koutecký, J.; Michl, J. *Angew. Chem., Int. Ed. Engl.* **1987**, *26*, 170.
(4) Platz, M. S., Ed. *Kinetics and spectroscopy of carbenes and biradicals*; Plenum Press: New York, 1990.
(5) Salem, L.; Rowland, C. *Angew. Chem., Int. Ed. Engl.* **1972**, *11*, 92.
(6) Coulson, C. A. *J. Chim. Phys.* **1948**, *45*, 243.
(7) Longuet-Higgins, H. C. *J. Chem. Phys.* **1950**, *18*, 265.
(8) Dowd, P. *J. Am. Chem. Soc.* **1966**, *88*, 2587.
(9) Slipchenko, L. V.; Krylov, A. I. *J. Chem. Phys.* **2003**, *118*, 6874.
(10) Wenthold, P. G.; Hu, J.; Squires, R. R.; Lineberger, W. C. *J. Am. Chem. Soc.* **1996**, *118*, 475.
(11) Wenthold, P. G.; Hu, J.; Squires, R. R.; Lineberger, W. C. *J. Am. Soc. Mass. Spectrom.* **1999**, *10*, 800.
(12) Borden, W. T.; Davidson, E. R. *J. Am. Chem. Soc.* **1977**, *99*, 4587.
(13) Ichino, T.; Villano, S. M.; Gianola, A. J.; Goebbert, D. J.; Velarde, L.; Sanov, A.; Blanksby, S. J.; Zhou, X.; Hrovat, D. A.; Borden, W. T.; Lineberger, W. C. *Angew. Chem., Int. Ed. Engl.* **2009**, *48*, 8509.
(14) Singleton, D. L.; Furuyama, S.; Cvetanović, R. J.; Irwin, R. S. *J. Chem. Phys.* **1975**, *63*, 1003.
(15) Cvetanović, R. J. *J. Phys. Chem. Ref. Data* **1987**, *16*, 261.
(16) Sabbah, H.; Biennier, L.; Sims, I. A.; Georgievskii, Y.; Klippenstein, S. J.; Smith, I. W. M. *Science* **2007**, *317*, 102.
(17) Taatjes, C. A.; Osborn, D. L.; Selby, T. M.; Meloni, G.; Trevitt, A. J.; Epifanovsky, E.; Krylov, A. I.; Sirjean, B.; Dames, E.; Wang, H. *J. Phys. Chem. A* **2010**, *114*, 3355.
(18) Slipchenko, L. V.; Krylov, A. I. *J. Chem. Phys.* **2002**, *117*, 4694.

(19) Krylov, A. I. *Chem. Phys. Lett.* **2001**, *338*, 375.
(20) Levchenko, S. V.; Krylov, A. I. *J. Chem. Phys.* **2004**, *120*, 175.
(21) Manohar, P. U.; Krylov, A. I. *J. Chem. Phys.* **2008**, *129*, 194105.
(22) Krylov, A. I. *Acc. Chem. Res.* **2006**, *39*, 83.
(23) Krylov, A. I. *Annu. Rev. Phys. Chem.* **2008**, *59*, 433.
(24) Cristian, A. M. C.; Shao, Y.; Krylov, A. I. *J. Phys. Chem. A* **2004**, *108*, 6581.
(25) Slipchenko, L. V.; Krylov, A. I. *J. Phys. Chem. A* **2006**, *110*, 291.
(26) Bettinger, H. F. *Angew. Chem., Int. Ed. Engl.* **2009**, *48*, 2.
(27) Schalley, C. A.; Blanksby, S.; Harvey, J. N.; Schröder, D.; Zummack, W.; Bowie, J. H.; Schwartz, H. *Eur. J. Org. Chem.* **1998**, 987.
(28) Osamura, Y.; Borden, W. T.; Morokuma, K. *J. Am. Chem. Soc.* **1984**, *106*, 5112.
(29) Coolidge, M. B.; Yamashita, K.; Morokuma, K.; Borden, W. T. *J. Am. Chem. Soc.* **1990**, *112*, 1751.
(30) Hess, B. A.; Smentek, L. *Eur. J. Org. Chem.* **1999**, *12*, 3363.
(31) Hrovat, D. A.; Rauk, A.; Sorensen, T. S.; Powell, H. K.; Borden, W. T. *J. Am. Chem. Soc.* **1996**, *118*, 4159.
(32) Hess, B. A.; Eckart, U.; Fabian, J. *J. Am. Chem. Soc.* **1998**, *120*, 12310.
(33) Lim, D. C.; Hrovat, D. S.; Borden, W. T.; Jorgensen, W. L. *J. Am. Chem. Soc.* **1994**, *116*, 3494.
(34) Polo, V.; Kraka, E.; Cremer, D. *Mol. Phys.* **2002**, *100*, 1771.
(35) Zhang, Y.; Yang, W. *J. Chem. Phys.* **1998**, *109*, 2604.
(36) Lundber, M.; Siegbahn, P. E. M. *J. Chem. Phys.* **2005**, *122*, 224103.
(37) Moriarty, N. W.; Lindh, R.; Karlsröm, G. *Chem. Phys. Lett.* **1998**, *289*, 442.
(38) We used $t(s) = 1/\nu(\mathrm{Hz})$ and $1\ \mathrm{Hz} = 3.336 \times 10^{-1}\ \mathrm{cm}^{-1}$ conversion factor to compute the broadening.
(39) The spectra are unpublished data from the authors' lab (University of Arizona). They are in agreement with those in ref 13.
(40) Helgaker, T.; Jørgensen, P.; Olsen, J. *Molecular electronic structure theory*; Wiley & Sons: New York, 2000.
(41) Raghavachari, K.; Trucks, G. W.; Pople, J. A.; Head-Gordon, M. *Chem. Phys. Lett.* **1989**, *157*, 479.
(42) Watts, J. D.; Gauss, J.; Bartlett, R. J. *J. Chem. Phys.* **1993**, *98*, 8718.
(43) Piecuch, P.; Włoch, M.; Gour, J. R.; Kinal, A. *Chem. Phys. Lett.* **2006**, *418*, 467.
(44) Sinha, D.; Mukhopadhyay, D.; Mukherjee, D. *Chem. Phys. Lett.* **1986**, *129*, 369.
(45) Sinha, D.; Mukhopadhya, D.; Chaudhuri, R.; Mukherjee, D. *Chem. Phys. Lett.* **1989**, *154*, 544.
(46) Chaudhuri, R.; Mukhopadhyay, D.; Mukherjee, D. *Chem. Phys. Lett.* **1989**, *162*, 393.
(47) Stanton, J. F.; Gauss, J. *J. Chem. Phys.* **1999**, *111*, 8785.
(48) Pieniazek, P. A.; Bradforth, S. E.; Krylov, A. I. *J. Chem. Phys.* **2008**, *129*, 074104.
(49) Pieniazek, P. A.; Arnstein, S. A.; Bradforth, S. E.; Krylov, A. I.; Sherrill, C. D. *J. Chem. Phys.* **2007**, *127*, 164110.
(50) Nooijen, M.; Bartlett, R. J. *J. Chem. Phys.* **1995**, *102*, 3629.
(51) Vanovschi, V.; Krylov, A. I.; Wenthold, P. G. *Theor. Chim. Acta* **2008**, *120*, 45.
(52) Kosloff, D.; Kosloff, R. *J. Comput. Phys.* **1983**, *52*, 35.
(53) Kosloff, R. *Annu. Rev. Phys. Chem.* **1994**, *45*, 145.
(54) Feit, M. D.; Fleck, J. A., Jr. *J. Chem. Phys.* **1983**, *78*, 301.
(55) Kosloff, R.; Kosloff, D. *J. Comput. Phys.* **1986**, *63*, 363.
(56) Mozhayskiy, V. A.; Krylov, A. I. *ez*Spectrum, http://iopenshell.usc.edu/downloads/.
(57) Shao, Y.; Molnar, L. F.; Jung, Y.; Kussmann, J.; Ochsenfeld, C.; Brown, S.; Gilbert, A. T. B.; Slipchenko, L. V.; Levchenko, S. V.; O'Neil, D. P., Jr.; Distasio, R. A.; Lochan, R. C.; Wang, T.; Beran, G. J. O.; Besley, N. A.; Herbert, J. M.; Lin, C. Y.; Van Voorhis, T.; Chien, S. H.; Sodt, A.; Steele, R. P.; Rassolov, V. A.; Maslen, P.; Korambath, P. P.; Adamson, R. D.; Austin, B.; Baker, J.; Bird, E. F. C.; Daschel, H.; Doerksen, R. J.; Drew, A.; Dunietz, B. D.; Dutoi, A. D.; Furlani, T. R.; Gwaltney, S. R.; Heyden, A.; Hirata, S.; Hsu, C.-P.; Kedziora, G. S.; Khalliulin, R. Z.; Klunziger, P.; Lee, A. M.; Liang, W. Z.; Lotan, I.; Nair, N.; Peters, B.; Proynov, E. I.; Pieniazek, P. A.; Rhee, Y. M.; Ritchie, J.; Rosta, E.; Sherrill, C. D.; Simmonett, A. C.; Subotnik, J. E.; Woodcock, H. L., III; Zhang, W.; Bell, A. T.; Chakraborty, A. K.; Chipman, D. M.; Keil, F. J.; Warshel, A.; Herhe, W. J.; Schaefer, H. F., III; Kong, J.; Krylov, A. I.; Gill, P. M. W.; Head-Gordon, M. *Phys. Chem. Chem. Phys.* **2006**, *8*, 3172.
(58) The $^3B_2-^3B_1$ adiabatic gap was computed as the energy difference between the EOM-IP-CCSD/aug-cc-pVTZ energies from the anion $^2A_2$ reference.
(59) ΔE refers to a computational strategy when the target energy gap is computed as a difference between the respective total energies, as opposed to the approaches formulated for direct calculation of energy differences, such as EOM-CC.
(60) Of course, such a flat PES may develop a shallow minima at a higher level of theory; however, it is unlikely that it can develop a well deep enough to accommodate at least one vibrational level.
(61) Kamarchik, E.; Kostko, O.; Bowman, J. M.; Ahmed, M.; Krylov, A. I. *J. Chem. Phys.* **2010**, *132*, 194311.

JP102183Z